Eur. Phys. J. B **16**, 719–728 (2000)

THE EUROPEAN PHYSICAL JOURNAL B

EDP Sciences

Periodic orbits in magnetic billiards

L.G.G.V. Dias da Silva[a] and M.A.M. de Aguiar[b]

Instituto de Física "Gleb Wataghin", Universidade Estadual de Campinas (UNICAMP), Caixa Postal 6165, 13083-970 Campinas, Brazil

Received 21 September 1999 and Received in final form 13 April 2000

Abstract. We propose a simple method to calculate periodic orbits in two-dimensional systems with no symbolic dynamics. The method is based on a line by line scan of the Poincaré surface of section and is particularly useful for billiards. We have applied it to the Square and Sinai's billiards subjected to a uniform orthogonal magnetic field and we obtained about 2000 orbits for both systems using absolutely no information about their symbolic dynamics.

PACS. 05.45.-a Nonlinear dynamics and nonlinear dynamical systems – 05.45.Pq Numerical simulations of chaotic models – 05.45.Mt Semiclassical chaos ("quantum chaos")

1 Introduction

The interest in the magnetic properties of mesoscopic systems has increased considerably in the last years. Many theoretical progresses have been recently achieved [1,2] motivated by exciting experiments involving trapped electrons in semiconductor heterostructures [3]. The behavior of these systems can be largely understood within the framework of semiclassical methods, where periodic orbits play an important role. Billiards in magnetic fields have been particularly useful in modeling two-dimensional electron gases confined by heterostructures in both regular and chaotic regimes [1,2,4]. Similar models have also been employed to describe the recent experiments on resonant tunneling diodes [5].

The basic connection between classical and quantum information is furnished by the Gutzwiller Trace Formula [6], relating the level density at energy E, $\rho(E)$, to a sum over all periodic orbits at that energy surface. An orbit with period τ contributes an oscillatory term to ρ with wave-length $2\pi\hbar/\tau$. A smoothed density, with resolution ϵ, can be obtained by taking into account only orbits with period smaller than $\hbar/\epsilon$. The trace formula is known to be divergent because of the exponential proliferation of periodic orbits and the so called entropy barrier [7]. Recent theoretical developments [8], however, have shown that the trace formula can be resummed in terms of a convergent (actually finite) series, the spectral determinant, whose zeros indicate the position of the energy levels. The classical ingredients for the spectral determinant are pseudo-orbits, linear combination of the actual periodic orbits. Although finite, the number of such orbits still increases exponentially fast with the energy and smoothed densities are still the best one can hope for at high energies. Famous applications of this semiclassical theory are the Hydrogen atom in a constant magnetic field [9] and the stadium billiard [10].

In a few special systems the periodic orbits can be computed with the help of a symbolic dynamics [11]. In these cases one can be sure to have all periodic orbits up to a certain value of period, action or length. Several new methods have recently been proposed which make explicit use of the symbolic code [12]. For generic systems, however, such symbolic dynamics does not exist and it becomes very hard to compute periodic orbits numerically. Most of the methods described in the literature for the computation of periodic orbits in generic systems are directly applicable only to maps with explicit equations (not, for instance, to a Poincaré section of a continuous flow). The simplest of those methods, introduced by de Vogeleare [13] and applied to the standard map by Greene [14] and to the oval billiard by Sieber [15], reduces the computation of periodic points to the calculation of roots of functions, which are essentially iterates of the functions describing the map. This works well for short orbits, but fails completely for long orbits. Another method applicable to explicit maps was proposed by Aubry [16], but it requires the integration of many differential equations and is very time consuming [17].

The best technique for finding periodic orbits, as far as convergence from trial orbits is concerned, is Newton's method [18–20]. Methods of this type, however, require the knowledge of an initial test orbit to start the convergence process. The calculation of these test orbits is actually the main task of any procedure based on Newton's method. Several different ways to generate test orbits (not relying on a symbolic code) can be found in the literature.

[a] e-mail: luisg@ifi.unicamp.br
[b] e-mail: aguiar@ifi.unicamp.br

These can be classified roughly into four groups: (a) interpolation from a known periodic orbit; (b) variation of a parameter; (c) Lyapunov exponent method and (d) area scan. The interpolation method is restricted to families of periodic orbits only, either stable [21] or close to homoclinic or heteroclinic orbits [18,19]. The second possibility, to vary a map parameter until the chaotic regions become small and then move the orbits back into the chaotic regions, fails to compute orbits born at tangent bifurcations [22]. The Lyapunov method applies to the calculation of stable orbits only [23]. Finally, in the area scan method one searchs for overlaps of a small phase-space region with its time evolved image [9,10,23]. Bisection methods have also been proposed as an alternative to the overlap criterion mentioned above [24–26]. In this case one also looks for roots of functions inside a small phase-space area, but, instead of using Newton's method to converge a trial solution, this small area is bisected according to certain criterions until the root is pinned with the desired accuracy.

In this article we present a simple modification of the area scan method which results in a very efficient way to compute periodic orbits in generic systems. As will become clear, this method is useful when one wants to calculate all the periodic orbits up to a certain period, and not just a few specific orbits. The method is presented in the next section. As applications we compute and study in Sections 3 and 4 the periodic orbits of the square and the Sinai's billiards subjected to a constant magnetic field perpendicular to the plane of the billiard. In both cases the classical dynamics changes continuously as the field intensity is varied [27] and the dynamics is generally mixed (partly chaotic and partly regular). The choice of these billiards as working models were motivated by their importance in the semiclassical calculations of the magnetic susceptibility in mesoscopic systems [1–4]. A second motivation is the role of bifurcations of periodic orbits in the susceptibility in some regimes [28], which cannot be described by a symbolic code.

2 The numerical calculation of periodic orbits

Our numerical method performs a search for periodic orbits directly on a Surface of Section, or Poincaré Map. Consider a conservative system whose dynamics can be described by a two-dimensional map of the form

$$\begin{cases} X_{n+1} = f(X_n, Y_n) \\ Y_{n+1} = g(X_n, Y_n) \end{cases}$$

where $f(X_n, Y_n)$ and $g(X_n, Y_n)$ are functions which depend on the dynamics and on the boundary conditions of the system. In the particular case of billiards, the coordinates X_n and Y_n are the Birkhoff coordinates at the n-th collision, namely the length l along the boundary where the collision takes place and $\cos\theta$, the cosine of the angle between the oriented boundary and the velocity right after the collision. A N point periodic orbit (N is discrete and, in the case of billiards, counts the number of bounces of the particle with the billiard boundary) is defined by a set of iterated points $(X_1, Y_1), (X_2, Y_2), ..., (X_N, Y_N)$, which belong to the map's domain, and with $(X_{N+1}, Y_{N+1}) = (X_1, Y_1)$.

We shall compute these orbits using a two-step algorithm that basically transforms the search for periodic points in the plane into two nearly one-dimensional searches. The first step is to find a special test orbit, *i.e.*, a set of points $(X_1^{(0)}, Y_1^{(0)}), (X_2^{(0)}, Y_2^{(0)}), ..., (X_N^{(0)}, Y_N^{(0)})$ which is a good approximation to the orbit we seek. The second step is to process this test-orbit with an iterative procedure, like Newton's method, to make it converge to the desired solution. As we shall see, this procedure becomes essentially one-dimensional for the test orbits provided by the first step, resulting in a fast and efficient algorithm.

2.1 Test-orbits: scanning the section line by line

A key point in the search for periodic orbits is to start with a good test-orbit. If no symbolic code is known the test-orbits themselves have to be computed numerically, and that is certainly the hardest part of the calculation.

We search for test-orbits by looking for their intersection with the surface of section. The simplest way to scan the surface of section is to divide it into small units, like squares or other geometric figures, and to evolve each of these units for N steps of the map. If the evolved unit has a non-empty intersection with the original unit we can produce an orbit which, after N steps, returns close to its initial point, being therefore a test-orbit. Any attempt to apply this procedure numerically for N large fails completely for chaotic maps. The main reason for this failure is that the area element becomes so thin and twisted that, numerically, one cannot distinguish it from a line. Moreover, since these 2-dimensional units are, for numerical purposes, a set of points distributed along their boundary, these points get apart from each other very fast under time evolution and, after a few iterations, the typical distance between neighboring points is larger that the size of the original unit. In this case it is hard to tell whether an intersection has occurred or not. Of course the exponential separation of points is unavoidable in chaotic maps. This problem can be minimized by propagating the points half the time forward and half the time backward if the map is invariant under time reversal (this is not the case of the magnetic billiards discussed in the next section). Lines and points are the only geometric structures that, in numerical simulations, survive a large number of iterations. Our approach, therefore, is based on a line-by-line scan of the surface of section, avoiding the inaccuracy imposed by the thinness of areas.

In the present case of magnetic billiards we have scanned the section by lines of constant $\cos\theta$, which we called previously Y, separated by a distance ΔY. The choice of these horizontal lines, instead of vertical or tilted lines, has to do with the fact that, for the square billiard and for $B \simeq 0$, two trajectories launched from the same

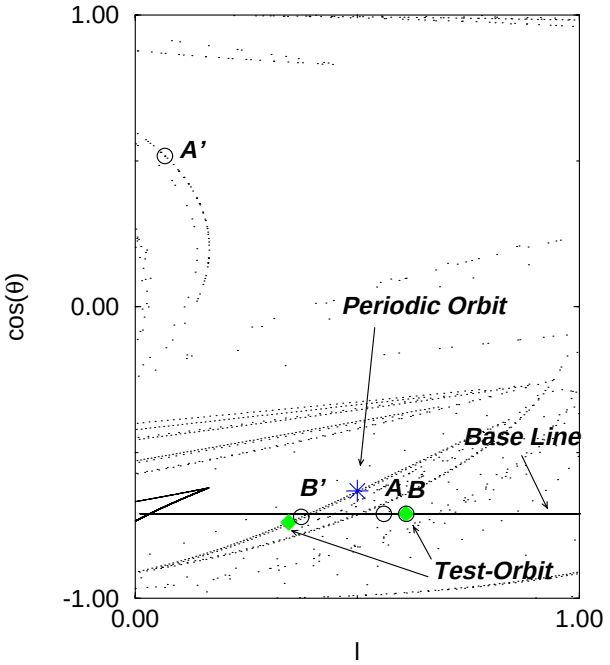

Fig. 1. Section map, l *versus* $\cos\theta$, for the Square with $B = 0.5$. The base line at $\cos\theta = -0.71$ is iterated 10 times and crosses itself several times. The points labeled A and B are mapped into A′ and B′. The diamond inside B is mapped into the other diamond close to B′ and constitutes a test-orbit.

point of the billiard boundary but at slightly different angles get apart much faster than two trajectories launched from slightly different points but with the same angle. Moreover, for $B \simeq 0$ the periodic orbits lie close to lines of constant Y and their stable and unstable manifolds are nearly parallel to the X axis, crossing at very small angles. For the Sinai's billiard the choice of lines is not important, as we shall see, but we have also used horizontal lines there. Each of these lines is represented by a set of points, separated by a distance ΔX, where X is the Birkhoff coordinate l. The accuracy of our search is then given by ΔX and ΔY: the smaller the Δ's, the more accurate is the search. In all our calculations, we have set $\Delta X = 0.0001$ (for a domain $0 < X < 1$) and $\Delta Y = 0.01$ ($-1 < Y < 1$). Each line is iterated N times and we check if the iterated line crosses the original line at some point. If it does, we use this crossing to generate a test of period N, as we describe bellow.

The construction of test orbits is illustrated in Figure 1 for the case of the square billiard with magnetic field intensity $B = 0.5$ (see Sect. 3 for details) and $N = 10$ iterations. The original line, referred in the figure as base line is crossed several times by its iterate. To make a clearer visualization of the process, let's consider only one of these crossings. We take two points on the base line which are at a distance $\Delta X = 0.05$ from each other, labeled A and B in Figure 1. After 10 iterations these points are mapped into A′ and B′ respectively. There is a point on the segment between A and B which is mapped very close to the base line. We could take the orbit starting at this point as a test-orbit (in this example the crossing point is very close to B′). We prefer, instead, to find the crossing point by linear interpolation between the two closer points on each side of the base line and transpose it back to the base line. This is shown as a little diamond inside the circle of point B. When iterated N times with the map this diamond goes into the other little diamond close to B′ and this is our test orbit. Notice that the $Y_{N+1}^{(0)} \simeq Y_1^{(0)}$ although $X_{N+1}^{(0)}$ is quite different from $X_1^{(0)}$. It turns out, however, that this is not a drawback, and we shall take advantage of this fact.

As mentioned above, the reason for our choice of horizontal lines has to do with the dynamics of the square billiard at low magnetic fields, $B \simeq 0$: if the initial and final point of the test orbit have nearly the same coordinate Y, they lie inside the narrow cones formed by the stable and unstable manifolds of a nearby periodic orbit. In this regions, the linearized equations used by the Newton's method correctly describes the dynamics and we expect very fast convergence. For the Sinai's billiard at low field intensities or for the square billiard at high B's, this argument does not apply and choice of horizontal or vertical lines is irrelevant.

2.2 The monodromy method for maps

Once a test-orbit has been obtained we must make it converge to a real periodic orbit. The test-orbit is given by a set of points $(X_1^{(0)}, Y_1^{(0)}), (X_2^{(0)}, Y_2^{(0)}), ..., (X_N^{(0)}, Y_N^{(0)})$ which are separated from the actual points of the periodic orbit by small corrections. We define $(X_{N+1}^{(0)}, Y_{N+1}^{(0)}) \equiv (X_1^{(0)}, Y_1^{(0)})$. In what follows we do not assume that the test-orbit is necessarily a solution of the map's equations, although it will be if generated by the method described in the last sub-section. For the purposes of this subsection the test-orbit can be just a suitable set of points on the map's domain. It is important to have this extra freedom if the system has a parameter that one wants to change, as illustrated in Section 4 with a study of bifurcations.

We want to compute $X_n^{(1)} = X_n^{(0)} + \delta X_n$ and $Y_n^{(1)} = Y_n^{(0)} + \delta Y_n$, the first order correction to $(X_n^{(0)}, Y_n^{(0)})$. We start by defining the functions $F(X,Y)$ and $G(X,Y)$ representing the map acting N times on the initial point (X,Y):

$$\begin{cases} X_{N+1} = f^N(X_1, Y_1) \equiv F(X_1, Y_1) \\ Y_{N+1} = g^N(X_1, Y_1) \equiv G(X_1, Y_1). \end{cases} \quad (1)$$

The N point periodic orbit satisfies $F(\bar{X}, \bar{Y}) = \bar{X}$ and $G(\bar{X}, \bar{Y}) = \bar{Y}$ and the problem reduces to that of finding fixed points of the 2-D map. The orbit is represented by its initial point $(X_1^{(0)}, Y_1^{(0)})$ that we call simply (X^0, Y^0). We look for corrections δX and δY such that $X^1 = X^0 + \delta X$ and $Y^1 = Y^0 + \delta Y$ satisfy $X^1 = F(X^1, Y^1)$

and $Y^1 = G(X^1, Y^1)$ to first order in δX and δY:

$$\begin{cases} F(X^1,Y^1) \approx F(X^0,Y^0) + \dfrac{\partial F}{\partial X^0}\,\delta X \\ \qquad\qquad + \dfrac{\partial F}{\partial Y^0}\,\delta Y \approx X^0 + \delta X \\ G(X^1,Y^1) \approx G(X^0,Y^0) + \dfrac{\partial G}{\partial X^0}\,\delta X \\ \qquad\qquad + \dfrac{\partial G}{\partial Y^0}\,\delta Y \approx Y^0 + \delta Y. \end{cases} \tag{2}$$

In matrix notation this becomes

$$\delta Z = M\,\delta Z + R \tag{3}$$

where

$$\delta Z \equiv \begin{pmatrix} \delta X \\ \delta Y \end{pmatrix};\; M \equiv \begin{pmatrix} \dfrac{\partial F}{\partial X^0} & \dfrac{\partial F}{\partial Y^0} \\ \dfrac{\partial G}{\partial X^0} & \dfrac{\partial G}{\partial Y^0} \end{pmatrix};\; R \equiv \begin{pmatrix} a \\ b \end{pmatrix} \tag{4}$$

and

$$\begin{aligned} a &= -X^0 + F(X^0,Y^0) \\ b &= -Y^0 + G(X^0,Y^0) \end{aligned} \tag{5}$$

measure how far from the periodic point the test-orbit is.

Solving for δZ gives:

$$\delta Z = (1 - M)^{-1}\, R. \tag{6}$$

This process can be iterated up to a given precision. The criterion we used in our numerical examples to stop the iteration is $E \equiv a^2 + b^2 \leq 10^{-10}$.

The method we have just described is essentially the monodromy method [20], with the difference that it is applied not along the orbit but directly between its initial and final points. For billiards this makes an enormous difference in terms of numerical convergence, since the errors in M are largely minimized. Once the test orbit converges to the periodic orbit, M becomes the monodromy matrix.

2.3 Convergence of test orbits

The advantage of a line-by-line search of the surface of section is that lines are easier to handle than areas, since they are one-dimensional objects. On the other hand, since lines do not cover a plane, almost no periodic orbit lies exactly on the lines used by the search algorithm, as the one shown in Figure 1. However, since we require the test orbit to end at the same line it started from, the Y distance (in the case of horizontal lines) from these points to the actual periodic point is always less than ΔY (the spacing between lines) for at least one of the lines used by the algorithm. As discussed above, the X distance between these initial and final points may, however, be large, especially if the Lyapunov exponent is large.

Let us consider the monodromy method applied to such a test orbit. We call $(\bar{X}, \bar{Y})$ the periodic point and, as before, (X^0, Y^0) and $(X^0_{N+1}, Y^0_{N+1}) = (F(X^0,Y^0), G(X^0,Y^0))$ the initial and final points of the test orbit. First we notice that, since both Y^0 and Y^0_{N+1} are close to $\bar{Y}$, the coefficient b in equation (5) is much smaller than a. We make this explicit by replacing $b \to \epsilon b$ where ϵ is a small parameter. Moreover, the correction δY is also smaller than δX and we may also write $\delta Y \to \epsilon \delta Y$. Then, the second of equations (2) says that $\frac{\partial G}{\partial X^0}$ must be of order ϵ as well.

With these considerations in mind, we can re-write equation (6) explicitly as

$$\begin{pmatrix} \delta X \\ \epsilon \delta Y \end{pmatrix} = \frac{1}{\det(M)} \begin{pmatrix} 1 - \dfrac{\partial G}{\partial Y^0} & -\dfrac{\partial F}{\partial Y^0} \\ -\epsilon \dfrac{\partial G}{\partial X^0} & 1 - \dfrac{\partial F}{\partial X^{)}} \end{pmatrix} \begin{pmatrix} a \\ \epsilon b \end{pmatrix} \tag{7}$$

or

$$\delta X = \left(1 - \frac{\partial F}{\partial X^0}\right)^{-1} a + O(\epsilon), \tag{8}$$

which is Newton's method for a one-dimensional map. Therefore, the imposition that one of the coordinates of the test orbit already nearly coincides with the periodic point reduces the convergence procedure to a nearly one-dimensional algorithm, increasing the efficiency of the method. After a few iterations the X distance between the test orbit and the periodic point, $|a|$, becomes comparable to the corresponding Y distance, $|b|$, and the procedure regains its 2D character. At this point, however, the test orbit is close to the periodic point in both X and Y.

In practical calculations we verify that some test orbits converge to periodic orbits whose Y coordinates are somewhat far from the initial Y_0. These periodic orbits are usually calculated several times by the algorithm, since many different test orbits converge to them, including the one whose horizontal line is very close to the orbit. This has to do in part with the fact that Newton's method is super convergent and it explains the assertion that the present method is useful when one is interested in all periodic orbits, since one cannot always forecast which periodic orbit will result from a given test orbit (see Ref. [29] for similar results using Newton's method). Notice that the individual orbits obtained by propagating a single horizontal line in the Sinai's billiard will not coincide with the orbits obtained by propagating, say, a vertical line. The final set of orbits, however, obtained after a full scan of the section, will coincide, no matter which type of lines are used.

One variation of the procedure for finding test orbits is to accept the test-orbit only if $|X^0_{N+1} - X^0_1| < \delta$ where δ is a control parameter. However, if δ is too small most test-orbits will be thrown away and a very large number of lines will be needed in order to generate acceptable orbits. In the examples studied here we found it more economical to just accept all test-orbits and let the convergence program decide whether or not they will converge to a real periodic solution.

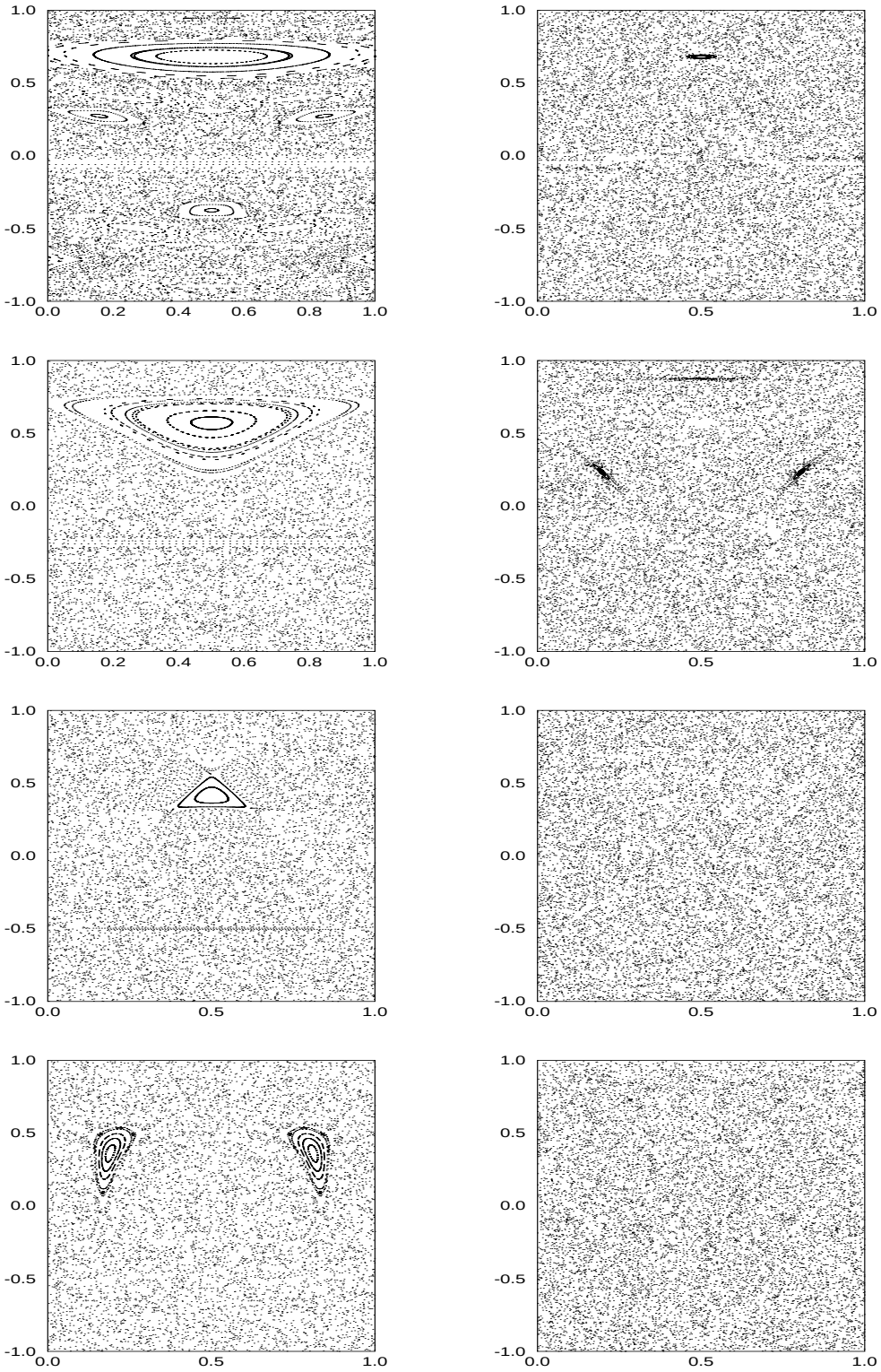

Fig. 2. Section maps for the square (left) and Sinai (right) billiards. From top to bottom the magnetic field is $B = 0.1$, 0.5, 1.0 and 3.0.

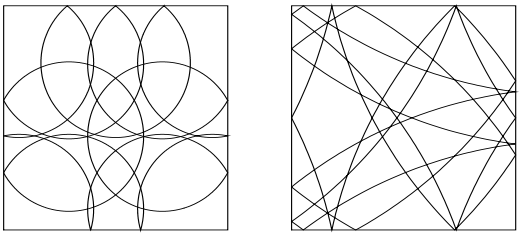

Fig. 3. Two examples of periodic orbits on the square billiard for $B = 3.0$ (left) and $B = 0.5$ (right).

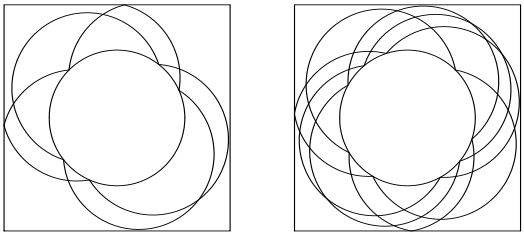

Fig. 4. Two examples of periodic orbits on the Sinai's billiard for $B = 3$.

3 Magnetic billiards

3.1 Description of the simulators: square and Sinai's billiards

We have focused our attention in two types of billiards, namely the square billiard and Sinai billiard, both subjected to an orthogonal magnetic field B. The trajectories of a charged particle inside these billiards are arcs of circles instead of straight line segments. The motion inside the billiard, for particle of unity mass and charge, is governed by the Hamiltonian

$$H = \frac{1}{2}\left[(p_x - yB)^2 + {p_y}^2\right]$$

and the orbit equation is a circle with radius $\sqrt{2E}/B$. When the particle hits the boundary, it is specularly deflected, just like the "free" ($B = 0$) case. The magnetic field B is our main parameter. We have fixed the energy on $E = 0.5$ so that the radius of the orbit is exactly $1/B$. When the magnetic field is increased the radius of the orbit decreases.

We have constructed numerical simulators for these systems using the following algorithm: given an initial condition consisting of a point along the boundary l_0 and an angle at which the trajectory is launched θ_0, we find the corresponding circular trajectory inside the billiard. We then check for collisions with the boundary: either with the external walls or, in the Sinai billiard, with the inner circle. At each collision, the orbit is specularly reflected and the next set of coordinates l_1, θ_1 is computed, generating another piece of circular trajectory. The map from l_0, $\cos\theta_0$ to l_1, $\cos\theta_1$ will be called the section map.

The side of the square in both billiards has been set to 1 and the radius of the inner circle in the Sinai's billiard has been fixed to 0.3 (arbitrary units).

3.2 Section maps and Birkhoff coordinates

Examples of section maps for both square and Sinai's billiards are shown in Figure 2 for $B = 0.1, 0.5, 1.0$ and 3.0. It is clear from these figures that neither the square billiard is integrable nor the Sinai's billiard is completely chaotic in the presence of the magnetic field. They become "mixed" systems in the sense that both types of behaviors are present on the Section map. The regions of regularity for the Sinai's billiard, however, are very small as compared to the non-regular ones. For the square billiard, on the other hand, large regular regions are clearly seen. For $B > 10$ the section map of the two billiards become identical since the orbits that hit the external boundary of the Sinai's billiard do not hit the inner circle and *vice-versa*.

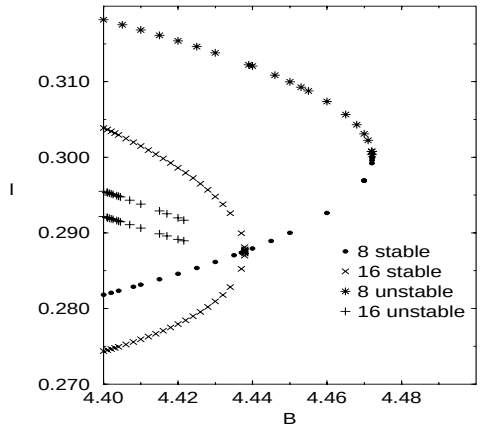

Fig. 5. Bifurcation diagram for the $4k$ family ($k = 2$). The Birkhoff l coordinate is plotted against the magnetic field.

4 Numerical results

We have successfully applied the method to the two billiards considered. We have obtained convergence of about 2 000 orbits, for various values of the magnetic field B.

Figure 3 shows two examples of periodic orbits for the square billiard. Part (a) shows a period 20 orbit computed for $B = 0.5$ and part (b) shows a period 11 orbit for $B = 3.0$. Figure 4 displays two examples of periodic orbits for Sinai's billiard computed for $B = 3.0$. Both orbits hit the outer boundary only twice while the inner boundary is hit 9 times in part (a) and 5 times in part (b). For each orbit we have also computed its action, period, length and the eigenvalues of the reduced Monodromy matrix.

4.1 Bifurcations

One important feature of the monodromy method is that it allows for the calculation of families of periodic orbits and to the study of their bifurcations. Given a periodic orbit (PO) at field intensity $B = \bar{B}$, we can compute

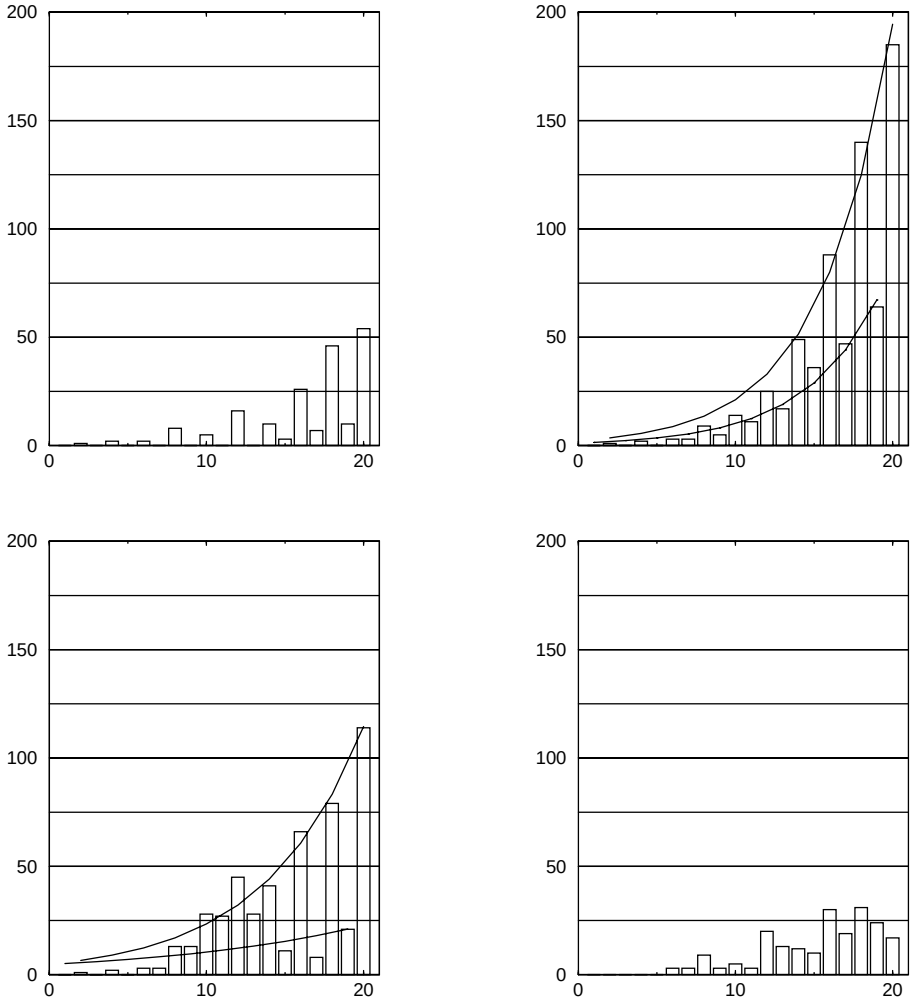

Fig. 6. Number of periodic orbits as a function of the number of bounces for the square billiard with magnetic field (from top left to bottom right) $B = 0.2$, 0.5, 0.8 and 3.0.

the periodic orbit at $B = \bar{B} + \delta B$ using the PO at $B = \bar{B}$ as a test-orbit. This is an example where the test orbit is not a solution of the map's equation for $B = \bar{B} + \delta B$. The recursive application of this procedure generates a one parameter family of periodic orbits. The eigenvalues of the Monodromy matrix along the family and the symmetry of the orbit give the relevant information about the bifurcations.

As an example we have studied the bifurcations of the 8-bounce orbit, which is also referred as a "$4k$ orbit" with $k = 2$ [30]. In Figure 5 we plot one of the eight Birkhoff l coordinates of the orbit as a function of B. The filled circles represent the stable branch of the family and the stars the unstable branch. These two branches coalesce at $B \simeq 4.4721$ in a tangent bifurcation. At $B \simeq 4.4379$ a period doubling bifurcation occurs along the stable branch, giving rise to two period 16 orbits. For each of these new orbits we plot the two Birkhoff l coordinates that branched from the plotted l of the period 8 orbit. The crosses show the stable bifurcated orbit and the *plus* symbol the unstable one (not shown all the way to the bifurcation point).

4.2 Histograms

In this subsection we show histograms of the number of calculated periodic orbits as a function of length and number of bounces for some values of the magnetic field B.

Figure 6 shows histograms of number of orbits as a function of number of bounces for the square billiard for $B = 0.2$, 0.5, 0.8 and 3.0. For these low values of the magnetic field we can see that there is a nearly exponential growth of the number of periodic orbits with the number of bounces N. This agrees with the expected results for the behavior of the number of orbits as a function of the period on regular and chaotic systems [31,32]. For regular systems, we expect $N_{\rm orbs}$, the number of orbits for a fixed period τ, to obey a power law for large τ, while for chaotic ones it grows exponentially with the period. In this case, the system is mixed. For the "free" square billiard ($B = 0$) there is a simple symbolic dynamics and it can be shown that $N_{\rm orbs}$ is a linear function of N for N large and that there are no orbits with N odd. For low values of B, there are two well-defined curves: one for N even and other for N odd. For larger values of B, like in $B = 3.0$, most

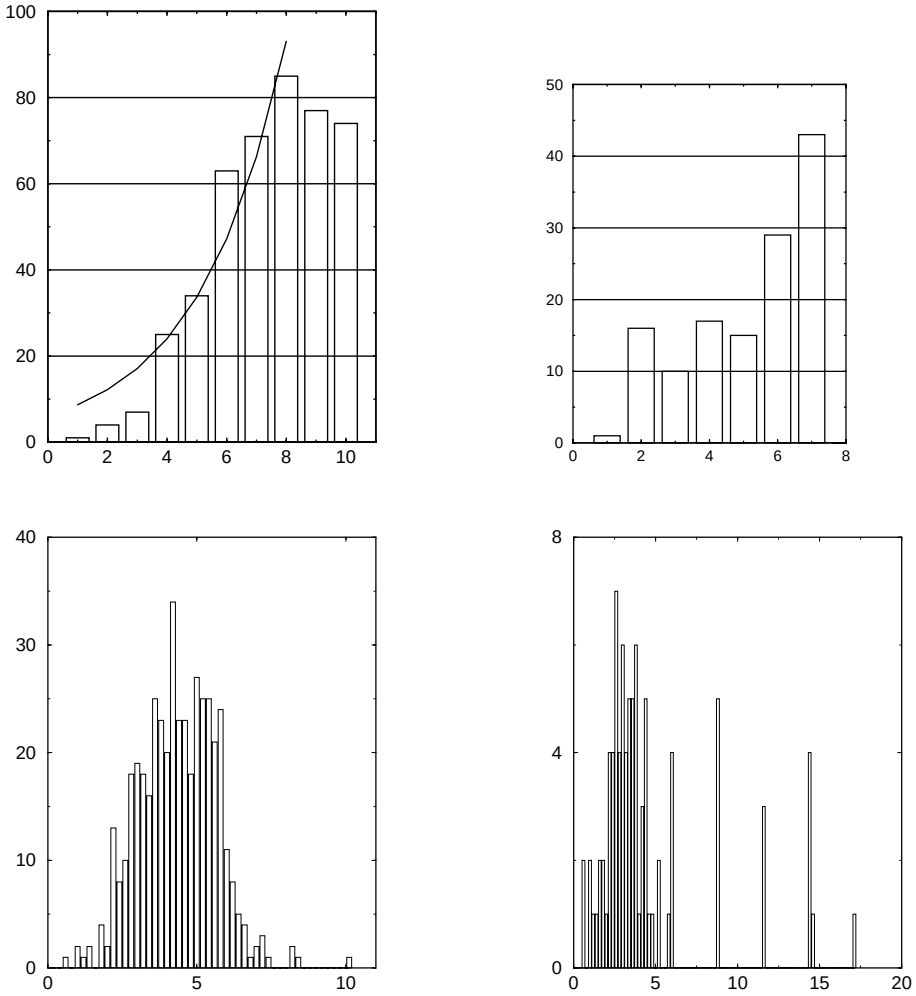

Fig. 7. Top: number of periodic orbits as a function of number of bounces for the Sinai's billiard and magnetic fields $B = 0.5$ (left) and 3.0 (right). Bottom: number of periodic orbits as a function of length for the Sinai's billiard and $B = 0.5$ (left) and 3.0 (right).

of the orbits hit the boundary a large number of times and there are very few low period orbits. The continuous lines in Figure 6 are an exponential fittings.

Figure 7 (top) shows similar histograms for the Sinai's billiard at $B = 0.5$ and $B = 3.0$ respectively. As we can see from these figures, there are much more short orbits in the Sinai's billiard than in the square billiard and there is no distinction between N even or odd. Once again, for B large the number of low period orbits decreases. The continuous line in Figure 7 for $B = 0.5$ is an exponential fitting.

The number of bounces with the outer boundary is not a good parameter to count orbits in the Sinai's billiard. The presence of the inner scattering disk may trap orbits inside the billiard [30]. These orbits have relatively long periods but they hit the external walls only a small number of times. The bottom part of Figure 7 shows histograms for the Sinai's billiard as a function of the length u of the orbits (which is proportional to the period). For $B = 0.5$ we see that the number of orbits increase with the length up to $u \simeq 4$ and then decreases fast. This is an indication that several orbits are missing for $u \geq 4$. Figure 8 shows an example of a trapped orbit with total length 17.22 that hits the external walls only twice. Histograms as a function of length for the square billiard do not add significant information and, therefore, are not shown.

5 Final remarks

We have presented an algorithm to calculate periodic orbits of two-dimensional maps based on the propagation of lines, instead of areas. The advantage of this procedure is that lines remain lines when iterated several times, whereas areas become thin so rapidly for chaotic maps that it becomes practically impossible to distinguish them from lines. The difficulties involved in finding the overlap between an original area element and resulting twisted filament are many. Finding the crossings of two lines

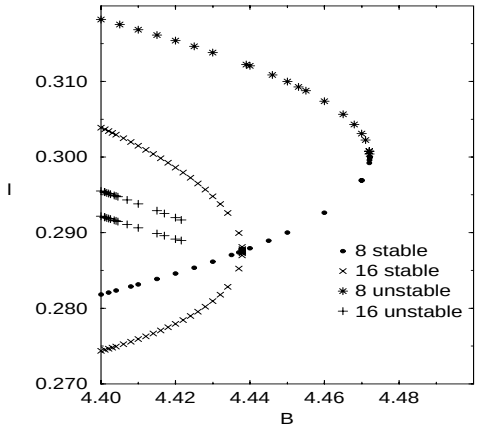

Fig. 8. Example of a trapped periodic orbit on the Sinai's billiard for $B = 3.0$. The orbit has approximate length of 17.22 and it hits the external walls only twice.

is, on the other hand, a simple matter. The disadvantage of this line-by-line search is that, obviously, lines do not cover the two dimensional domain of the map. Therefore, almost no periodic orbits will lie exactly on the lines used by the search algorithm, like the one shown in Figure 1. Nevertheless, it is easy to see that the existence of a periodic point of period N close to a line implies in the crossing of this line and its Nth iterate.

The line search method provides test-orbits. These are special approximations to the periodic orbits where the initial point has one of its coordinates (Y in our examples) very close to the corresponding coordinate of the final point, which is also close to that of the periodic orbit. These test-orbits have been inserted on a monodromy procedure, based on the Newton's method, to make them converge to real periodic orbits. The role of Newton's method in its first iterations is to act basically on the "bad coordinate" (X in our case). This nearly one-dimensional character of Newton's method is responsible for its efficiency in converging the test orbits. As discussed in Section 2, the procedure present here is useful when one is interested in all periodic orbits, since one cannot always predict which periodic orbit will result from a given test orbit. On the other hand, if a symbolic code is not available, the only way to verify that all orbits of period N have been found is to refine the numerical search including more lines until no more new orbits are encountered. As a test to our method we have computed the periodic orbits of the square billiard for low magnetic fields, where a simple symbolic code holds approximately for the periodic orbits with even number of bounces. For the case of $B = 0.2$ we found all orbits indicated by the symbolic code up to $N = 10$. At this value of N several periodic orbits not contained in the symbolic code have also been detected. For larger N's the code is not reliable and no agreement can be expected.

Finally we remark that this line-by-line search has also been applied with success to calculate periodic orbits of a smooth Hamiltonian system with two degrees of freedom [33]. In this case the Poincaré map has to be constructed numerically integrating Hamilton's equation and the calculation becomes, of course, lengthy. These results will be published elsewhere.

This paper was partly supported by FAPESP, CNPq and Finep.

References

1. D. Ullmo, K. Richter, R. Jalabert, Phys. Rev. Lett. **74**, 383 (1995); O. Agam, J. Phys. I France **4**, 697 (1994); F. von Oppen, Phys. Rev. B **50**, 17151 (1994); S.D. Prado, M.A.M. de Aguiar, J.P. Keating, R. Egydio de Carvalho, J. Phys. A **27**, 6091 (1994).
2. D. Ullmo, H. Baranger, K. Richter, Felix von Oppen, R. Jalabert, Phy. Rev. Lett. **80**, 895 (1998).
3. L.P. Lévy *et al.*, Physica B **189**, 204 (1993); C.M. Marcus *et al.*, Phys. Rev. Lett. **69**, 506 (1992); D. Weiss *et al.*, Phys. Rev. Lett. **66**, 2790 (1991).
4. D. Weiss *et al.*, Phys. Rev. Lett. **70**, 4118 (1993); R. Fleischmann, T. Geisel, R. Ketzmerick, Phys. Rev. Lett. **68**, 1367 (1992); R.A. Jalabert, H.U. Baranger, A.D. Stone, Phys. Rev. Lett. **65**, 2442 (1990).
5. T.M. Fromhold *et al.*, Phys. Rev. Lett. **72**, 2608 (1994); E.E. Narimanov, D.D. Stone, Phys. Rev. Lett. **80**, 49 (1998); T. Monteiro, Phys. Rev. E **58**, R2704 (1998).
6. M.C. Gutzwiller, *Chaos in Classical and Quantum Mechanics* (Springer-Verlag, New York, 1990).
7. A. Voros, J. Phys. A **21**, 686 (1988); B. Georgeot, R.E. Prange, in *Proceedings of the 4th Drexel Symposium on Quantum Nonintegrability*, edited by D.H. Feng, B.L. Hu (International Press, 1997).
8. M.V. Berry, J.P. Keating, J. Phys. A **23**, 4839 (1990); M.V. Berry, J.P. Keating, Proc. Roy. Soc. (London) A **437**, 151 (1992); E.B. Bogomolny, Nonlinearity **5**, 805 (1992); B. Georgeot, R.E. Prange, Phys. Rev. Lett. **74**, 2851 (1995).
9. D. Delande, J.C. Gay, Phys. Rev. Lett. **57**, 2006 (1986); K. Dupret, D. Delande, Phys. Rev. A **57**, 1257 (1996).
10. E.J. Heller, Phys. Rev. Lett. **53**, 1515 (1984); S. Tomosovic, E.J. Heller, Phys. Rev. Lett. **67**, 664 (1991).
11. P. Cvitanović, B. Eckhardt, Phys. Rev. Lett. **63**, 823 (1989); E. Doron, U. Smilansky, Phys. Rev. Lett. **68**, 1255 (1992).
12. O. Biham, M. Kvale, Phys. Rev. A **46**, 6334 (1992); K.T. Hansen, Phys. Rev. E **52**, 2388 (1995); A. Backer, H.R. Dullin, J. Math. Phys. A **30**, 1991 (1997).
13. R. de Vogelaere, *Contributions to the theory of nonlinear oscillations*, edited by S. Lefschetz (Princeton U. Press, New Jersey, 1958), Vol. IV, p. 53.
14. J. Greene, J. Math. Phys. **20**, 1183 (1979).
15. M. Sieber, J. Phys. A **30**, 4563 (1997).
16. S. Aubry, Physica D **7**, 240 (1983).
17. R.S. Mackay, J.D. Meiss, I.C. Percival, Physica D **27**, 1 (1987).
18. B. Mestel, I.C. Percival, Physica D **24**, 172 (1987).
19. Q. Chen, J.D. Meiss, I.C. Percival, Physica D **29**, 143 (1987).
20. M. Baranger, K.T.R. Davies, Ann. Phys. (N.Y.) **177**, 330 (1987).

21. M.A.M. de Aguiar, M. Baranger, Ann. Phys. (N.Y.) **186**, 355 (1988).
22. M.A.M. de Aguiar, C.P. Malta, Phys. Rev. A **42**, 2438 (1990).
23. D. Grobgeld, E. Pollak, J. Zakrzewski, Physica D **56**, 368 (1992).
24. J.M. Greene, J. Comp. Phys. **98**, 194 (1992).
25. M.N. Vrahatis, J. Comp. Phys. **119**, 105 (1995).
26. L. Drossos, O. Ragos, M.N. Vrahatis, T. Bountis, Phys. Rev. E **53**, 1206 (1996).
27. M. Robnik, M.V. Berry, J. Phys. A **18**, 1361 (1985); M. Robnik, in *Nonlinear Phenomena and Chaos*, edited by S. Sakar (Adam Hilger, 1986), p. 303.
28. S.D. Prado, M.A.M. de Aguiar, Phys. Rev. E **54**, 1369-1377 (1996).
29. R. Marcinek, E. Pollak, J. Chem. Phys. **100**, 5894 (1994).
30. N. Berglund, A. Hansen, E.H. Hauge, J. Piasecki, Phys. Rev. Lett. **77**, 2149-2153 (1996).
31. V.I. Arnold, *Mathematical Methods for Classical Mechanics* (Springer, Berlim, 1989).
32. A.M.O. de Almeida, *Sistemas Hamiltonianos: Caos e Quantização* (Unicamp, Campinas, 1991).
33. F.A. Bajay, Master's Thesis, Universidade Estadual de Campinas, IFGW, 1992 (in Portuguese).